



**Formation of peptide-based oligomers in dimethylsulfoxide:  
Identifying the precursor of fibril formation**

Journal:	<i>Soft Matter</i>
Manuscript ID	SM-ART-01-2020-000035.R2
Article Type:	Paper
Date Submitted by the Author:	29-Jun-2020
Complete List of Authors:	<p>Levine, Matthew; Drexel University, Chemistry            Ghosh, Moumita; Indian Association for the Cultivation of Science,            Department of Biological Chemistry; Tel Aviv University, Department of            Oral Biology            Hennessy, Nathan; Drexel University, Chemistry            DiGuseppi, David; Drexel University, Department of Chemistry; Drexel            University            Schweitzer-Stenner, Reinhard; Drexel University, Chemistry            Adler-Abramovich, Lihi; Tel Aviv University, Department of Oral Biology            Hesser, Morgan; Drexel University, Department of Chemistry</p>

## ARTICLE

## Formation of peptide-based oligomers in dimethylsulfoxide: Identifying the precursor of fibril formation

Received 00th January 20xx,  
Accepted 00th January 20xx

DOI: 10.1039/x0xx00000x

Matthew S. Levine<sup>a,‡</sup>, Moumita Ghosh<sup>b,‡</sup>, Morgan Hesser<sup>a</sup>, Nathan Hennessy<sup>c</sup>, David M. DiGuseppi<sup>a</sup>, Lihl Adler-Abramovich<sup>b\*</sup>, and Reinhard Schweitzer-Stenner<sup>a\*</sup>

The well-studied dipeptide fluorenylmethoxycarbonyl-di-phenylalanine (FmocFF) forms a rigid hydrogel upon dissolving in dimethylsulfoxide (DMSO) and dilution in H<sub>2</sub>O. Here, we explored the pre-aggregation of the peptide in pure DMSO by vibrational spectroscopies, X-ray powder diffraction and dynamic light scattering. Our results show an equilibrium between a dominant population of amorphous oligomers (on a length scale of 2 nm) and a small number of protofibrils/fibrils (on a length scale of 30 nm in the centimolar and of 200 nm in the sub-molar region). To probe the mechanism underlying the formation of these protofilaments, we measured the <sup>1</sup>H-NMR, IR and visible Raman spectra of DMSO containing different FmocFF concentrations, ranging between 10 and 300 mM. Our data reveal that interpeptide hydrogen bonding leads to the self-assembly of FmocFF in the centimolar region, while  $\pi$ - $\pi$  stacking between Fmoc-groups is observed above 100 mM. The high <sup>3</sup>J(H<sup>N</sup>H<sup>C $\alpha$</sup> ) coupling constant of the N-terminal amide proton indicates that the Fmoc end-cap of the peptide locks the N-terminal residue into a conformational ensemble centered at a  $\phi$ -value of *ca.* -120°, which corresponds to a parallel  $\beta$ -sheet type conformation. The <sup>3</sup>J(H<sup>N</sup>H<sup>C $\alpha$</sup> ) coupling constant of the C-terminal residue is indicative of a polyproline II (pPII)/  $\beta$ , mixture. Our results suggest that the gelation of FmocFF caused by the addition of a small amount of water to DMSO mixtures is facilitated by the formation of disordered protofibrils in pure DMSO.

### Introduction

Over the last 15 years, low molecular weight peptides have emerged as building blocks of remarkable supramolecular structures. While earlier work suggested that peptide self-assembly into fibrils requires a minimal length of *ca.* 10-15 amino acid residues,<sup>1-4</sup> more recent studies demonstrated that oligopeptides with 2 or 3 amino acid residue and even individual amino acids can self-assemble into nanotubes or hydrogels, depending on the experimental conditions.<sup>5-9</sup> Generally, the aggregation of very short peptides into higher order structures requires a high degree of aromaticity of the amino acid side chains,<sup>10-14</sup> even though some exceptions are noteworthy.<sup>15,16</sup> Phenylalanine has emerged as the amino acid with the highest aggregation propensity.<sup>17,18</sup> The self-assembly capability of phenylalanine-containing oligopeptides can be further enhanced if the N-terminus is replaced by the aromatic fluorenylmethoxycarbonyl (Fmoc) group.<sup>13,14,19-22</sup> Moreover, even Fmoc-protected amino acids were shown to form ordered

structures at the nano-scale.<sup>23-26</sup> Alternatively, short peptides can be linked to functionalized carbon hydrogen chains to facilitate self-assembly and gelation.<sup>27</sup> Some modified tri-phenylalanine peptides composed of mixtures of L- and D-amino acid residues have also been shown to be effective gelators.<sup>28</sup>

One of the most prominent representatives of the group of self-assembling phenylalanine-based oligopeptides is Fmoc-diphenylalanine (FmocFF).<sup>13,14,21,22,29-33</sup> The formation of a 3D self-supporting hydrogel by the FmocFF peptide was demonstrated by two common protocols. One option starts with FmocFF dissolved in polar or organic solvents, such as DMSO, methanol, and hexafluoroisopropanol, followed by dilution in water.<sup>13,22,30</sup> This produces a sample spanning network of fibrils on a micrometer scale with fibril thicknesses on a 10<sup>-8</sup> m scale.<sup>22</sup> The formed gels showed high storage modulus (G') values, between 10<sup>3</sup> and 5·10<sup>4</sup> Pa.<sup>21,13</sup> The hydrogel line is linear in a log-log diagram of water and peptide fraction.<sup>22</sup> Alternatively, gelation can be induced by dissolving the peptide in an alkaline aqueous solution followed by titration of the sample back to acidic values.<sup>34</sup> Multiple lines of evidence suggest that the underlying fibrils of the hydrogel phases constitute  $\beta$ -sheet structures stabilized by  $\pi$ - $\pi$ -stacking between Fmoc groups and phenylalanine side chains in adjacent peptides.<sup>13,35</sup>

The initial state of FmocFF in DMSO is frequently used as the starting point for gelation experiments. Reported data clearly suggest that even the addition of a small amount of water (a mole fraction of approximately 0.15) can induce gelation if the

<sup>a</sup> Department of Chemistry, Drexel University, 3141 Chestnut Street, Philadelphia, PA 19104, USA. Email: rschweitzer-stenner@drexel.edu

<sup>b</sup> Department of Oral Biology, The Goldschleger School of Dental Medicine, Sackler Faculty of Medicine, and The Center for Nanoscience and Nanotechnology, Tel Aviv University, Tel Aviv 69978, Israel. Email: LihlA@tauex.tau.ac.il

<sup>‡</sup> These authors contributed equally

<sup>†</sup> Electronic Supplementary Information (ESI) available: Microscopy images, IR related data, chemical shift temperature dependencies, simulation of amide I VCD and OR profiles, IR spectra of DMSO-water mixtures. See DOI: 10.1039/x0xx00000x

volume fraction of the peptide is close to 0.1.<sup>22</sup> Yet, the exact initial conditions, namely whether FmocFF is monomeric in DMSO or whether it forms small assemblies or oligomers which serve as a nucleus for the fibrilization process that precedes the formation of the gel phase, is still unclear. Identifying the formation of FmocFF assemblies in DMSO and their isolation are extremely challenging as these oligomers are only transient intermediates of the fibrilization process. Here, we combine infrared (IR), dynamic light scattering (DLS), vibrational circular dichroism (VCD), Raman and <sup>1</sup>H NMR spectroscopy to demonstrate the self-assembly of FmocFF in DMSO into elongated protofibrils. This assembly is mediated by  $\pi$ - $\pi$  interactions between Fmoc groups and hydrogen bonding involving all functional groups of the peptide. Interestingly, the formed protofibrils are intrinsically disordered and do not comprise of ordered  $\beta$ -sheets.

## Experimental

### Materials

Fmoc-di-phenylalanine was purchased from Bachem (CAS 4015688 Lot 1068270) and used without further purification. DMSO and dDMSO (i.e. DMSO with deuterated methyl groups), both <sup>3</sup> 99.9% purity, were purchased from Sigma Aldrich

### NMR experiments

For NMR experiments, the sample was composed of 10% dDMSO and 90% DMSO. 750  $\mu$ L of the final solution was transferred to the NMR tube. Temperature-dependent <sup>1</sup>H-NMR spectra were recorded for all Fmoc-FF samples using a Varian 500 MHz FT-NMR with a 5 mm HCN triple resonance probe. The v.6.1 Varian software was used for processing of all spectra. The sample was set at a spin of 20 Hz, and spectra were collected starting at 25 °C while increasing by 5 °C for each measurement with a maximum temperature of 80 °C. Only for a peptide concentration of 200 mM, due to laboratory conditions, the measurements were started at 30 °C. 32 scans were collected for each spectrum. The fid files were opened in MestReC software, which was used for the Fourier transforms and phase correction. NMR peaks of interest were fitted to a Lorentzian band profile. <sup>3</sup>J(H<sup>N</sup>H<sup>C $\alpha$</sup> ) constants were obtained as a function of temperature by employing the strategy previously described by Toal et al.<sup>36</sup>

### IR and VCD experiments

dDMSO was used for all VCD/IR experiments. IR and VCD spectra were measured on a BioTools Chiral IR and were loaded in a 121  $\mu$ m CaF<sub>2</sub> biocell from BioTools. VCD measures the difference between the left- and right handed absorptivity of infrared bands assignable to molecular vibrations.<sup>37</sup> Hence, it probes the local chirality of functional groups, which in peptides are mostly induced by the chiral environment of individual peptide groups. Spectra with a resolution of 8 cm<sup>-1</sup> and scan speed of 83 scans per minute were collected using the Grams/IR

7.00 software (Thermo Galactic). VCD spectra were recorded over a period of 10 hours. The temperature of the sample was maintained by a BioTools water-cooled temperature controller. The IR spectra were not solvent-corrected in order to detect any changes of the solvent bands. Part of the observed spectra were decomposed into individual Gaussian bands using our MULTIFIT program.<sup>38</sup> All VCD spectra were baseline-corrected.

### Raman spectroscopy

Aliquots of FmocFF in dDMSO were loaded onto a microslide with a single concavity and covered with a glass coverslip. The slide was positioned onto an Olympus BH2-UMA microscope and spectra were obtained using a 442 nm excitation with a He-Cd laser (model IK 4601R-E, Kimmon Electric, USA). Using the Renishaw WIRE software (version 1.330), four spectra with a range of 500-1800cm<sup>-1</sup> were obtained and subsequently averaged for each sample.

### X-ray Diffraction (XRD)

100  $\mu$ L aliquot of FmocFF dissolved in DMSO (200 mM) and small portion of FmocFF hydrogels were placed on glass slides and allowed to air dry at ambient conditions. The XRD pattern was collected using a Bruker's D8 Discover Diffractometer; the applied set-up was a  $\theta$ : $\theta$  Bragg-Brentano geometry, the source was a copper anode and the detector was a LYNXEYE XE linear detector. The diffraction patterns were collected between 4 and 40°2 $\theta$  with step 0.02°2 $\theta$  at 1 second per step.

### Dynamic Light Scattering (DLS) measurements

FmocFF was dissolved in DMSO (200 mM). The size distribution of the FmocFF assemblies was measured using Zeta PALS DLS (Malvern Instruments Ltd. Worcestershire, UK) with appropriate refractive index settings. The temperature was maintained at 25 °C during the measurement. The reported data are averages of triplicate samples. Concentration-dependent DLS was performed in a similar manner using FmocFF solutions of 10, 30, 70 and 200 mM in DMSO.

## Results and discussion

The first part of this section reports the results of spectroscopic studies (NMR, IR and VCD) which explored whether or not intensities and positions of spectroscopic markers of FmocFF change if the peptide concentration is varied. A measurable concentration dependence of spectroscopic parameters is an unambiguous indicator of peptide aggregation.<sup>39</sup> The spectroscopic data are augmented by results from x-ray diffraction and dynamic light scattering experiments which shed some light on the structure and size of peptide aggregates.

### NMR spectroscopy

We studied different concentrations of FmocFF in DMSO at 30 °C using <sup>1</sup>H NMR analysis. Figure S1 shows the spectrum of FmocFF

in the region between 7.0 and 8.3 ppm. The spectra of 200 mM FmocFF recorded at different temperatures are depicted in Figure S2. The two amide proton doublets are clearly distinct. The chemical shift of the C-terminal signal was 8.23 ppm at 25°C while the N-terminal proton signal was observed at 7.55 ppm.<sup>40</sup> Other signals in this region were assignable to the protons of the Fmoc group.<sup>41</sup>

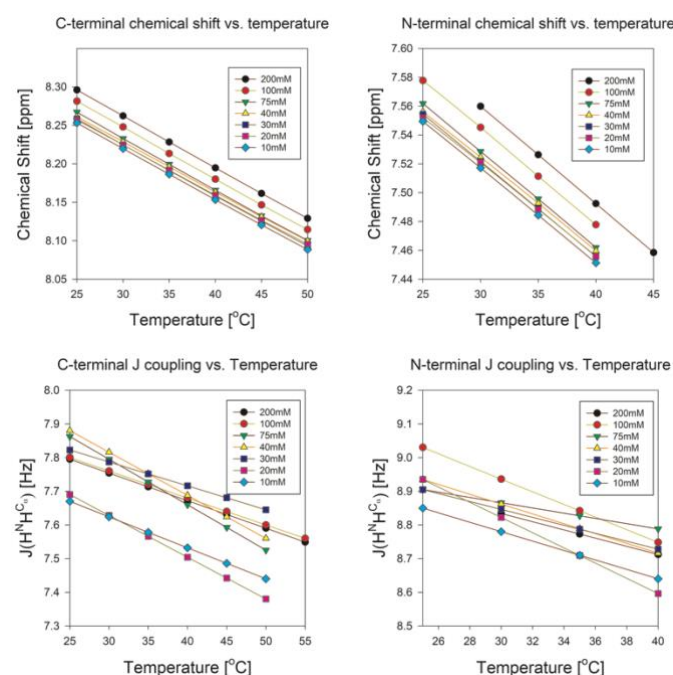


**Figure 1:**  $^1\text{H}$  NMR analysis of FmocFF in DMSO. Temperature dependence of the chemical shift and the  $^3J(\text{H}^1\text{H}^{13}\text{C})$  coupling constants of the C-terminal and N-terminal amide protons. Measurements were performed for the indicated concentrations of FmocFF in DMSO.

Figures 1A and 1B depict the temperature dependence of the chemical shifts of both amide proton signals for different peptide concentrations. As expected, both signals shifted upfield with increasing temperature. In addition, we observed a small yet consistent downfield shift with increasing concentration (from 7.52 ppm at 10 mM to 7.56 ppm at 200 M at 30°C). Figure S3 presents the changes of the amide proton shift with increasing concentrations with respect to the chemical shift measured for 10 mM peptide. Figure S3 also compares these changes with the concentration dependence of three CH signals assignable to two Fmoc and a phenylalanine substituent (Figure S4). These plots reveal that the concentration dependences of the amide proton resonances is very similar and much more pronounced than those of the CH resonances.

The observed downfield shift of amide proton signals is probably indicative of a slightly stronger hydrogen bonding due to a switch from peptide-solvent to inter peptide hydrogen bonding. In principle, an increase of the temperature coefficient

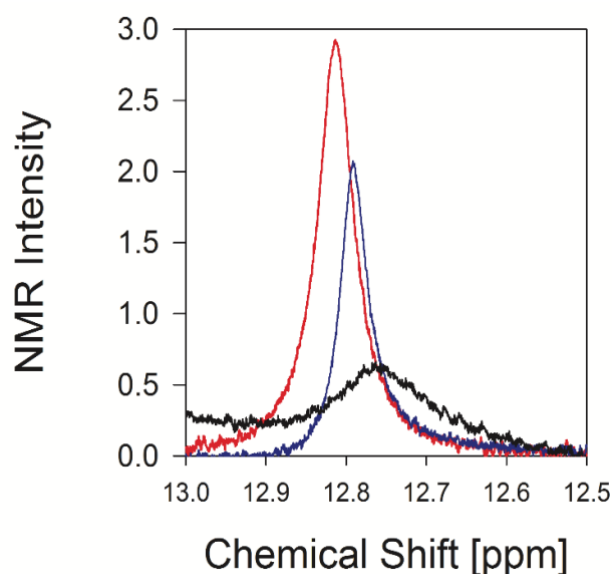


**Figure 2:**  $^1\text{H}$  NMR spectrum of FmocFF in the 12.5-13 ppm region.  $^1\text{H}$  NMR spectrum of FmocFF in the 12.5-13 ppm region measured with the indicated peptide concentrations. The peak assignable to the OH group in carboxylate dimers appears at 12.75 ppm in the spectrum of 75 mM FmocFF (black). It shifts upfield and becomes sharper with increasing peptide concentration (blue: 100 mM; red: 200 mM).

of chemical shifts (i.e. shift towards less negative values) is expected in such a case.<sup>42</sup> We observe in Figure 1, the downfield shift of the chemical shifts of both amide protons with increasing concentration is not accompanied by an increase of the temperature coefficient. Taken together, the concentration and temperature dependence of the amide proton signals indicate a dynamic exchange of hydrogen bonding either between FmocFF-DMSO and FmocFF-FmocFF complexes or between different FmocFF oligomers. Gonzalez and Chavez observed that the chemical shift of the acetamide proton in DMSO exhibits a concentration dependence with a concentration coefficient of 0.14 ppm/M.<sup>43</sup> The downfield shifts of the C- and N-terminal protons observed for a concentration increase up to 190 mM indicate a value of 0.16 ppm/M for both protons, which is very close to the above acetamide value. We therefore concluded that the concentration dependence of the amide proton chemical shifts displayed in Figures 1 and S3 reflects a transition from peptide – DMSO to inter peptide hydrogen bonding in the centimolar region. Herein, the inter peptide hydrogen bonding might be advantageous due to potential involvement of all carbonyl groups (peptide and C-terminal). This includes the amide group of the two peptide groups, the hydroxyl group and the C=O group of the C-terminal carboxylic acid end group. Moreover, the ether oxygen of the carbamate group can act as a hydrogen bonding acceptor. The multiplicity of hydrogen bond acceptors (4) and donors (3) might allow the formation of a variety of amorphous aggregates.

Figures 1C and D display the temperature dependence of the  $^3J(\text{HNH}^{\text{C}\alpha})$  coupling constants (termed  $^3J$  constant in the following) of the two amide protons for different peptide concentrations. For the 10 mM sample at room temperature, the C-terminal  $^3J$  value was observed at 7.7 Hz, similar to the value of 7.5 Hz obtained for cationic GFG in water.<sup>44</sup> This value was found to be indicative of a conformational distribution comprising 45 mol% pII, 45 mol%  $\beta_t$  and 10 mol%  $\gamma$ - and  $\beta$ -turn type conformations. Upon increasing the peptide concentration, this value started to increase at 40 mM, with a maximal value of 7.9 Hz observed at 200 mM. However, the  $^3J$ -value did not increase monotonously with peptide concentration. The corresponding N-terminal values were consistently higher (8.7 Hz for 10 mM, 9.02 Hz for 100 mM, and 8.3 Hz for 200 mM). For all peptide concentrations, the  $^3J$  values decreased with increasing temperature. This is distinctly different from our observations for unblocked tri- and tetrapeptides,<sup>45,46</sup> where the slopes are always positive.

The particularly high  $^3J$ -values of the N-terminal proton were very close to the maximal value of 10 Hz that this constant would reach if the residue was locked into a conformation with  $\phi = -120^\circ$  (cf. the Karplus plot reported by Graf et al.<sup>47</sup>). The obtained values are therefore indicative of a conformational distribution dominated by  $\beta_t$ -type conformations, which has  $\phi$  values similar to the canonical parallel  $\beta$ -conformation, but larger  $\psi$ -values.<sup>48,49</sup> In order to estimate the mole fraction of this conformation, we used the previously described algorithm<sup>50</sup> to calculate the  $^3J$  coupling constant for different conformational distributions involving  $\beta_t$ , pII and turn-like conformations.<sup>48</sup> The results suggest that 80-90 mol% of the N-terminal residue conformation must be of  $\beta_t$ -type in order to yield a  $^3J$ -value above 8.5 Hz. This implies that the neighboring Fmoc group locks the N-terminal residue mostly into a  $\beta_t$ -type conformation. This results in a conformational rigidity which might facilitate the formation of inter peptide hydrogen bonding. In contrast, the C-terminal  $^3J$ -coupling suggests that the corresponding phenylalanine residue mostly resembles the balanced pII/ $\beta_t$  distributions that we observed for GFG and other GxG peptides with aromatic residues at the central position.<sup>51</sup>

The observed decrease of  $^3J$  with increasing temperature suggests a slightly more disordered structure for the N-terminus. This observation could be indicative of either a population of  $\beta$ -strand conformations with a larger negative  $\phi$ -value or an increased population of pII. The latter option would be unusual, since pII is generally enthalpically stabilized and therefore not favored at high temperatures.<sup>45</sup> However, it is possible that FmocFF becomes conformationally more flexible at high temperatures which reduces its capability to affect the conformational flexibility of the N-terminal residue. This allows the phenylalanine residue to adopt a conformational distribution which resembles more its intrinsic propensities. A change of the conformational distribution of the N-terminal residue could then be transduced to the C-terminus via nearest neighbor interactions.<sup>46</sup>

Thus far, we have identified solely inter peptide hydrogen bonding between C=O and NH groups as a mode of peptide-

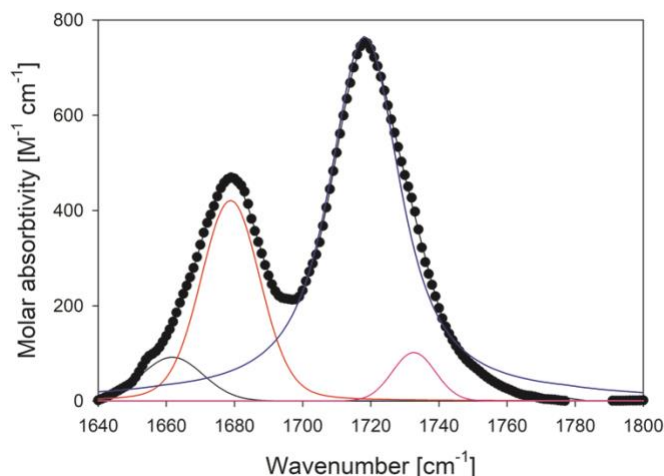


**Figure 3:** IR spectrum of 100 mM FmocFF in DMSO in the region between 1640 and 1800  $\text{cm}^{-1}$ . The experimental spectrum (filled circles) was decomposed into Gaussian bands at 1661 (black) and 1679 (red), a Voigtian band at 1718 (blue) and another Gaussian band at 1732  $\text{cm}^{-1}$  (pink).

peptide interaction. In addition, interactions between the terminal groups may also be possible. Protonated carboxylate acid groups can form dimers via hydrogen bonding. The proton signal of the OH proton is generally very weak and can be found just around 12 ppm. The formation of dimers enhances the signal, increases its intensity and considerably shifts it downfield.<sup>52</sup> Figure 2 shows the  $^1\text{H}$  NMR spectrum of FmocFF in the region between 12 and 14 ppm for three different peptide concentrations. At 75 mM, a broad peak emerged at 12.75 ppm which increased and narrowed with increasing concentration. This observation is a clear indication for the formation of FmocFF aggregates via intermolecular hydrogen bonding between carboxylate acid groups. The temperature dependence of the chemical shift shown in Figure S5 suggests a temperature coefficient of ca.  $-5.3$  ppb/ $^\circ\text{C}$  which is slightly larger (i.e. less negative) than values of protons that are not hydrogen bonded. Thus, the data suggest that FmocFF aggregation involves hydrogen bonding between COOH groups at a concentration above 70 mM.

### IR and VCD spectroscopy

Next, we analyzed FmocFF in DMSO using IR spectroscopy. Figure 3 shows the region between 1630 and 1800  $\text{cm}^{-1}$  of the IR spectrum of 100 mM FmocFF in dDMSO. We used the Multifit software (cf. Material and Methods) to heuristically decompose the entire spectrum into Gaussian bands. The two dominant bands at 1679 and 1718  $\text{cm}^{-1}$  can be assigned to the amide I modes of the C-terminal peptide and the carbamate group, respectively. This assignment is corroborated by Fleming *et al.* who reported wavenumber positions of 1669 and 1708  $\text{cm}^{-1}$  for the C-terminal and carbamate amide I of FmocAA in methanol.<sup>53</sup> The high wavenumber position of the latter reflects the carbamate character of the N-terminal linkage between the Fmoc group and the phenylalanine residue. The slightly higher

wavenumber of the carbamate C=O band in DMSO reflects the absence of hydrogen bonding to the carbonyl group by the solvent or (weaker) interpeptide hydrogen bonding. In spite of the difference between this linkage and a conventional terminal peptide residue, we continue to use the term amide I for the vibrational mode the eigenvector of which we expected to be dominated by a C=O stretching contribution. In order to check this conjecture, we performed a density functional theory calculation for FmocFF *in vacuo* (both amide protons were replaced by deuterons) on a BLYP G31G\*\* level of theory. The vibrational wavenumbers were calculated after geometry optimization in the upper left quadrant of the Ramachandran plot. We obtained a structure with  $\phi=-88.34^\circ$  and  $\psi=135^\circ$  for the central phenylalanine residue of the peptide, which lies in the middle between  $\beta_t$  and the canonical pPII conformation. The vibrational analysis for this conformation yielded two heavily mixed vibrations at 1789 and 1788  $\text{cm}^{-1}$ , which were both predominantly C=O stretching modes. Interestingly, a semi-empirical AM1 calculation yielded a much more accurate description of the amide I wavenumber splitting, namely a vibration at 2035  $\text{cm}^{-1}$  for the carbamate amide I' and 1994  $\text{cm}^{-1}$  for the C-terminal amide I'.

The wavenumber difference between the two amide I modes is rather large (40  $\text{cm}^{-1}$ ) compared to values generally observed for unblocked tripeptides or blocked dipeptides,<sup>36,54</sup> mostly caused by the additional redshift of the carbamate amide I mode. The occurrence of two C-terminal amide I bands (i.e. a weak band at 1661  $\text{cm}^{-1}$  in addition to the 1679  $\text{cm}^{-1}$  band) was reminiscent of our earlier observation of an amide I doublet in the spectrum of N-methylacetamide in DMSO which we assigned to species with and without hydrogen bonding between the NH group and the sulfoxide group of the solvent.<sup>55</sup> It is noteworthy that the integrated intensity of the carbamate amide I band was substantially larger than that of the C-terminal amide I band. In unblocked tripeptides, both bands mostly exhibit similar intensities.<sup>48</sup> The weak band at 1733  $\text{cm}^{-1}$  was assigned to the C=O group of the C-terminal carboxylic acid group.<sup>56</sup> This band is generally significantly broader and exhibits less peak intensity than amide I' bands of tripeptides.<sup>57</sup>

We measured the IR spectrum of FmocFF in dDMSO at different solute concentrations, decomposed the spectra as described above and plotted the integrated band intensities as a function of peptide concentration (Figure S6). It should be noted that these bands might actually represent bands of overlapping excitonic transitions. The observed spectral changes were moderate. The intensities of the amide I band at 1718  $\text{cm}^{-1}$  and of the CO stretching band of the carboxylate acid group decreased with increasing peptide concentration. The weaker bands at 1661 and 1678  $\text{cm}^{-1}$  were subject to some scattering. The former clearly increased with peptide concentration while the latter was almost concentration independent in the limit of accuracy. The changes of wavenumbers were marginal. The 1678  $\text{cm}^{-1}$  band slightly downshifted (2  $\text{cm}^{-1}$ ) with increasing peptide concentration, while the carbamate amide I shifted up to the same extent. The

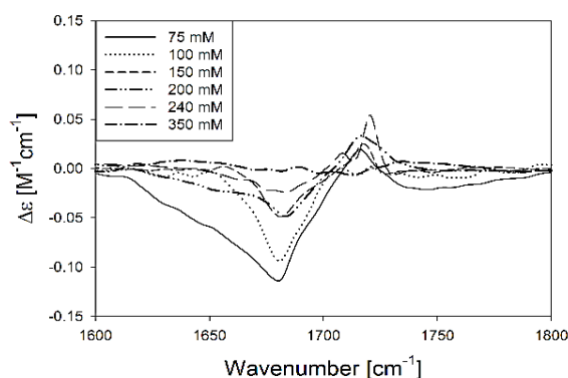


**Figure 4:** VCD spectrum of FmocFF in dDMSO between 1600 and 1800  $\text{cm}^{-1}$  measured for the indicated peptide concentration.

observed redistribution of intensities indicates an onset or of some change in the state of aggregation in the centimolar region.

Importantly, the band assignment described thus far does not take into account the possibility of excitonic coupling between peptide groups in oligomers and protofibrils. As argued below, the concentration dependence of the corresponding VCD spectrum actually suggests further complexity where the observed spectral profile of amide I should be considered as the envelope of excitonic bands. This result from intermolecular vibrational coupling between amide I modes in peptide aggregates.

The VCD spectrum of 200 mM FmocFF in dDMSO is displayed in Figure 4. It exhibited a rather pronounced negative symmetric couplet. The negative peak was broadened towards its low wavenumber side. In unblocked cationic GFG in water, the phenylalanine residue nearly adopts a 50:50 mixture of pPII and  $\beta_t$ -type conformations centered at  $\phi$  values of  $-80^\circ$  and  $-110^\circ$  in the Ramachandran plot, respectively.<sup>48</sup> The corresponding VCD signal carried half of the rotational strength of the FmocFF signal displayed in Figure 3. This observation was rather surprising in view of the fact that the larger wavenumber difference between the two amide I' modes of FmocFF leads to a decrease of the quantum mechanical mixing between the respective vibrational states and thus to a lower rotational strength.<sup>54</sup> The observed couplet therefore suggests a rather strong excitonic coupling between the carbamate and peptide (C-terminal) amide I which could be either intramolecular in peptide monomers, intermolecular in peptide aggregates, or a combination of both. If soluble oligomers or even protofibrils are present in the investigated sample, the VCD, and to a lesser extent the IR spectrum, are expected to depend on peptide concentration. Non-amorphous protofibrils are generally but not exclusively formed as aggregates of  $\beta$ -sheet tapes. Thus they give rise to IR-spectra with the amide I band substantially downshifted due to in-phase vibrational coupling between amide I modes in adjacent strands.<sup>58–60</sup> The corresponding VCD signal would be very weak ( $10^{-2} \text{ M}^{-1}\text{cm}^{-1}\text{residue}^{-1}$ ) unless the  $\beta$ -sheets are helically twisted which can lead to an enhancement

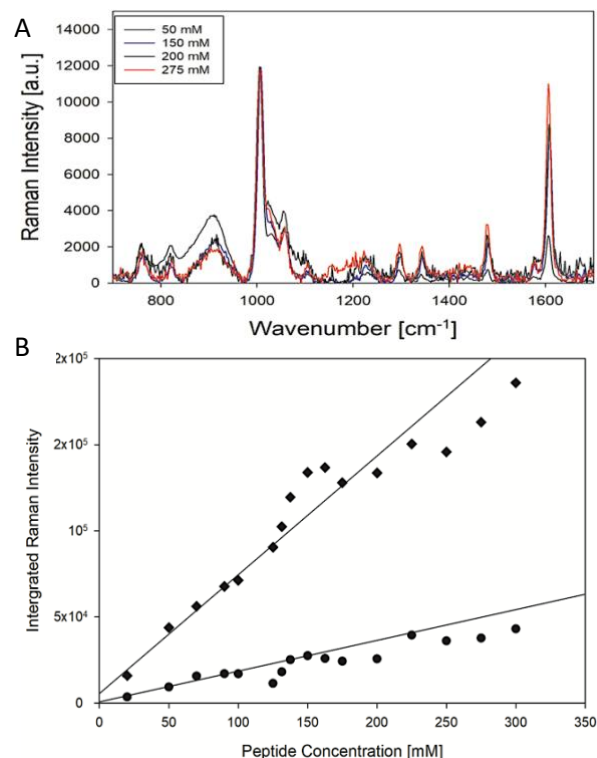
of the VCD signal by up to two orders of magnitude.<sup>15,61</sup> Increasing or decreasing the length of protofilaments due to dissociation and association processes would hardly affect the IR spectrum in the amide I region. It could significantly affect the respective rotational strength if the underlying  $\beta$ -sheets are helically twisted.<sup>61,62</sup> In the case of disordered aggregates, the long-range order, which leads to the amide I downshift and VCD enhancement, can be expected to be absent. Based on the recent observation of amorphous aggregates of cationic GAG tripeptides,<sup>63</sup> we expected the amide I profile in the IR spectrum of FmocFF in DMSO to resemble more or less the monomeric peptide, while the rotational strength might become somewhat enhanced.<sup>16</sup> Moreover, we expected the VCD signal to change with varying peptide concentration.

Figure 4 reveals that the amide I VCD indeed varied with peptide concentration, but in a somewhat unexpected way. At 300 mM, the VCD signal is almost undetectable. A rather modest decrease of the peptide concentration in the sub-molar region (240–150 mM) lead to the appearance of a pronounced negative couplet. This VCD signal became even more intense and negatively biased in the centimolar region. Negative bias is generally indicative of intrinsic magnetic transition dipole moments due to slightly non-planar peptide group or the occurrence of ring currents.<sup>64</sup> Such ring currents can be produced within hydrogen bonding networks. The profile of the negative Cotton band observed at 75 mM and to an even larger extent at 50 mM suggests a distribution of delocalized excitonic states with different rotational strength. This phenomenon is different to the overlap of two Gaussian bands that emerged from our heuristic spectral decomposition in Figure 3. This difference can easily be explained by slight changes of the relative orientations of peptides in amorphous oligomers and protofilaments. Generally, our VCD spectra suggest somewhat different modes of FmocFF self-assembly in the centimolar and sub-molar region. Peptide aggregates formed in the former seem to be actually less chiral than the ones formed at lower peptide concentrations.

### Raman spectroscopy

Next, we studied different concentrations of FmocFF in DMSO using Raman spectroscopy (Figure 5A). All spectra were normalized to the DMSO band at 1008  $\text{cm}^{-1}$ <sup>65</sup> to eliminate the influence of slight differences between optical alignments. The dominant bands in the spectrum could all be assigned to ring modes of Fmoc. We focused on two bands positioned at 1479 and 1606  $\text{cm}^{-1}$ .<sup>66</sup> The wavenumber position of the former did not change with temperature, the latter seemed to exhibit a small blue shift of 2  $\text{cm}^{-1}$ , in the limit of experimental accuracy, at 70 mM and higher concentrations. Changes of the intensities were much more significant. If no aggregation was affecting the aromatic groups of the peptide, all Fmoc and phenylalanine bands should increase linearly with peptide concentration. However, as depicted in Figure 5B, this is not the case for both bands. To illustrate and identify deviations from linearity, we subjected only the five data points obtained at the lowest concentrations to a linear regression. For the 1479  $\text{cm}^{-1}$  band,

we observed minor yet systematic deviations at higher concentrations above 160 mM. The 1606  $\text{cm}^{-1}$  intensity clearly shows a non-linear and non-monotonous behavior. Above 130 mM, we observed a larger than linear increase until a maximum was reached at ca. 160 mM. After a slight decrease, the intensity increased again but the slope was significantly less than the



**Figure 5: Raman analysis of FmocFF peptide.** (A) Visible Raman spectra of the indicated concentration of FmocFF in DMSO. The spectra were normalized to the DMSO band at 1008  $\text{cm}^{-1}$ . (B) Integrated Raman intensities of the band at 1479  $\text{cm}^{-1}$  (diamonds) and 1606  $\text{cm}^{-1}$  (full circles) plotted as a function of peptide concentration. The solid line is the result of a linear regression to the data points obtained for the five lowest concentrations.

initial one. Since the intensities do not vary *in sync* we can exclude systematic experimental errors. The observed changes might be attributed to  $\pi$ - $\pi$  stacking between Fmoc groups that affects the 1606  $\text{cm}^{-1}$  band more than the 1479  $\text{cm}^{-1}$  band. However, the literature is not clear about how  $\pi$ - $\pi$  stacking affects the C=C ring mode of aromatic groups. Raman experiments probing the  $\pi$ - $\pi$  stacking in the self-assembly of hIAPP<sub>22-29</sub> indicate a very slight redshift and a drastic decrease of the respective Raman band's intensity.<sup>67</sup> This would be qualitatively, though not quantitatively, consistent with the drop in intensity at 170 mM (Figure 5).

### XRD and DLS Analysis

FmocFF dissolves readily in DMSO to form a clear solution (Figure S7A), however upon subsequent dilution in water, it forms a three-dimensional self-supporting hydrogel (Figure S7B).<sup>13,32,40,68</sup> We performed powder XRD analysis of dried FmocFF following its dissolution in DMSO at 200 mM and of

dried FmocFF hydrogels prepared in DMSO/water and compared the spectra with the previously reported FmocFF crystals in acetone/water.<sup>28</sup> The spectra did not show crystallinity in both FmocFF in DMSO and in FmocFF hydrogel in DMSO/water (Figure S7C).

We used light scattering techniques to further study the FmocFF peptide in pure DMSO solution. DLS analysis of FmocFF in DMSO showed a strong intensity in the range of ~200-500 nm, with a maximal intensity at 250 nm (Figure 6). We further performed a concentration dependent DLS analysis over a range of 10-200 mM to confirm the formation of nanostructures. A broad intensity peak at ~50 nm was observed for the 10 mM, 30 mM and 70 mM peptide solutions, while the 200 mM sample showed peaks at ~200 nm (Figure S8).

The size distributions depicted in the left column of Figure S8 correspond to the correlation functions  $G^{(1)}(\tau)$  plots in the right column. They were calculated from the experimentally obtained  $G^{(2)}(\tau)$  correlation function by the Siegert relation. The  $G^{(1)}$  function obtained for 10 and 30 mM could be fitted with two exponential functions augmented by a first order cumulant term. The first one which accounts for most of the correlation decay corresponds to the single peak in the distribution function. The second one was introduced to account for the slowly decaying baseline above 1000  $\mu$ s. The  $G^{(1)}$  functions obtained for 70 and 200 mM had to be fitted with three exponential functions augmented by a first and second order (for 200 mM) cumulant expansion.<sup>69</sup> The two distributions in Figure S8E and G correspond to the two exponential decays in a time window below 10<sup>4</sup>  $\mu$ s. For all concentrations, we ignored any contributions on longer time scales for the distribution analysis because of the statistical uncertainties of the corresponding fitting parameters.

Based on the DLS and spectroscopic data we suggest the following scenario. At 10 mM the sample is dominated by a distribution of short fibrils or filaments with an average size of ca. 30 nm. The small peak at 4 nm might not be statistically significant. At 30 mM a second peak at 2 nm emerges. The value is too large for peptide monomers for which we estimated an average end to end distance of maximal 0.95 nm for a fully extended peptide. For the average  $\beta_1$ -conformation derived from  $^3J(N^H C^H\alpha)$  values (*vide supra*) the estimated end to end distance is 9Å. The peak at 30 nm is therefore assignable to peptide oligomers (dimers or trimer). The fraction of oligomers is much larger than the intensity of the peaks suggests. Since the intensity scales with the 6<sup>th</sup> power of the diameter (Rayleigh scattering) the number of 30 nm fibrils becomes actually negligible compared with the number of oligomers (~10<sup>-8</sup> of the 2 nm clusters). If one considers the fibrils/clusters as spheres (which is an oversimplification) one estimates that ca. 0.1% of the peptides are incorporated in fibrils or protofibrils. At 70 mM the relative fraction of protofibril/fibril population slightly decreases. At 200 mM the 30 nm peak disappears and is replaced by a rather sharp peak at 200 nm. This means that a very small fraction of peptides assembles in larger fibrils (10<sup>-8</sup>). Our spectroscopic results might shed some light on this

unexpected behavior. Figure S9 shows the concentration dependence of the  $^3J(N^H C^H\alpha)$  values displayed of FmocFF as measured at 25° C. For the C-terminal constant the value increases with peptide concentration until it reaches a maximum at 50 mM from where it slightly decays above 70 mM. Changes of the N-terminal constant are less pronounced and the data scatter somewhat for concentrations above 40 mM. This is not surprising since the J-coupling values are close to a maximum of the Karplus curve where changes of  $\phi$  translate into less significant changes of  $^3J(N^H C^H\alpha)$  (*vide supra*). The increase of the coupling constant values at low peptide concentration coincides nicely with the distribution change indicated by the DLS data. The concentration dependence of the COOH signal in Figure 2, the changes of the VCD amide I signal (Figure 4) and the non-linearity of the Raman intensities above 70 and 100 mM, respectively, indicate some change in the sub-molar region which most likely involves hydrogen bonding between C-terminal carboxylate groups. This new mode of peptide-peptide interaction might even facilitate the formation

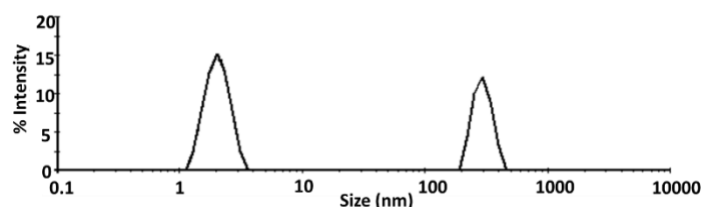


**Figure 6: Dynamic light scattering.** DLS measurement of FmocFF solution in DMSO at a concentration of 200 mM.

of the small number of longer fibrils obtained for 200 mM FmocFF samples. The conversion of short fibrils/protofibrils to oligomers in the low centimolar range is indicative of an off-pathway aggregation which can slow down fibrilization significantly. Only at high peptide concentration fibril formation moves into the time window of our experiments. The chemical shift data discussed above reveal that the oligomers are dynamic entities with continuous hydrogen bond exchange.

#### Probing the water content of peptide samples

We further aimed to verify that the formation of protofibrils obtained in this study was not facilitated by the presence of a small amount of water. The DMSO was purchased at a purity of  $\geq 99.9\%$ . In order to check confirm this, we inspected the IR spectrum of the purchased DMSO and of DMSO samples into which 0.1 and 0.2 mol% water was added. Even upon the addition of 0.1 mol%, which would correspond to the minimal sample purity guaranteed, the water bands dominated the spectrum in the region between 1600 and 1700  $\text{cm}^{-1}$  and between 3000 and 3750  $\text{cm}^{-1}$  (Figure S9). These spectroscopic data confirm that with regard to H<sub>2</sub>O, the purity of the DMSO used in this study was at least an order of magnitude higher than the value guaranteed by the vendor. A mol % of 0.01 H<sub>2</sub>O would correspond to a concentration of 0.55 mM, which lies well below the peptide concentrations investigated. We therefore conclude that H<sub>2</sub>O cannot be responsible for the observed self-assembly of peptides.

## Summary and conclusions

This paper addresses the question whether FmocFF can pre-aggregate in DMSO. Clarifying this issue is key to understand why this peptide self-assembles into a sample spanning network of fibrils upon the addition of even a very small amount of water. We report, for the first time, the formation of self-assembled nanostructures by the FmocFF peptide in pure DMSO solution. We found that the concentration dependence of  $^1\text{H}$  NMR, IR, VCD and Raman spectra reflects the peptide's self-assembly into some type of supramolecular amorphous structures. The process starts in the low centimolar regime of peptide concentration (Figure S4). However, as indicated by our Raman, VCD and NMR results (Figures 1, 3, 4 and 6), the type of aggregation and thus the relative orientation of peptide groups in the respective supramolecular structures are different in the centimolar and low sub-molar region. This notion is further corroborated by the DLS results. The Raman and NMR data indicate that the transition from the former to the later involves (possibly  $\pi$ - $\pi$ ) interactions between the terminal Fmoc groups as well as hydrogen bonding between the COOH group of the C-terminus and hydrogen bonding acceptor groups of the peptide.

The observation that the NMR, Raman, IR and VCD spectra of FmocFF in DMSO depend on the peptide's concentration indicates that the peptides self-assemble into some type of oligomers and nanostructures. Since none of the two amide I bands appear at a position indicative of a classical  $\beta$ -strand conformation, we conclude that the overall structure of the formed protofibrils is disordered. However, the enhancement of the VCD of the amide I modes relative to the very weak signal expected for an FmocFF monomer suggests that some type of local order must exist in order to allow the focusing of rotational strength in a limited number of excitonic transitions.<sup>70</sup> The size of protofibrils suggests lateral assembly of peptide which could involve  $\pi$ - $\pi$  interactions and hydrogen bonding between carboxylic acid groups. The NMR data suggest that individual peptides are structurally more constrained at the N-terminal than at the C-terminal side. Altogether, our data are indicative of aggregation taking place in the centimolar region. The change of the chemical shifts of the amide protons and of the amide I intensities suggests changes of interpeptide hydrogen bonding between CO and NH groups in the 10-50 mM region and additional interpeptide hydrogen bonding between COOH groups above 70 mM. Increasing the concentration above 100 mM results in aggregation mediated by (possibly  $\pi$ - $\pi$ ) interactions between Fmoc groups. The unusual temperature dependence of  $^3\text{J}(\text{H}^{\text{N}}\text{H}^{\text{C}\alpha})$  indicates that conformational distributions might become more heterogeneous at high temperatures.

To conclude, our results suggest that FmocFF dissolution in DMSO results in the formation of disordered oligomers and to a much more limited extend of protofibrils. The oligomer formation seems to be off path which serve as the precursors for fibril formation in water. It remains to be seen which of the two population provides the starting point for large-scale self-assembly of peptides in the presence of water.

## Conflicts of interest

There are no conflicts to declare.

## Acknowledgements

The research in the Biospectroscopy Laboratory at Drexel University was in part supported by a grant from the National Science Foundation to R.S.S. (DMR-1707770). Nathan Hennessy was an undergraduate exchange student from Sheffield University, UK. The work in the Adler-Abramovich group was partially supported by the ISRAEL SCIENCE FOUNDATION (grant No. 1732/17) (L.A.A.). We thank Davide Levy for help with XRD analyses, and the Chaoul Center for Nanoscale Systems of Tel Aviv University for the use of instruments and staff assistance. We thank the members of the Adler-Abramovich group and Biospectroscopy Laboratory for helpful discussions. R.S.S. would like to thank Ms. Bridget Milorey for her assistance with Figures 1 and S1 of the manuscript.

## References

- 1 S. E. Blondelle, B. Forood, R. A. Houghten and E. PerezPaya, *Biochemistry*, 1997, **36**, 8393–8400.
- 2 T. Measey and R. Schweitzer-Stenner, *J. Am. Chem. Soc.*, 2006, **128**, 13324–13325.
- 3 T. J. Measey, R. Schweitzer-Stenner and V. Uversky, in *Protein and Peptide Folding, Misfolding and Non-Folding*, ed. R. Schweitzer-Stenner, Wiley & Sons, Hoboken, 2012, pp. 309–350.
- 4 J. P. Schneider, D. J. Pochan, B. Ozbas, K. Rajagopal, L. Pakstis and J. Kretsinger, *J. Am. Chem. Soc.*, 2002, **124**, 15030–15037.
- 5 L. Adler-Abramovich and E. Gazit, *Chem. Soc. Rev.*, 2014, **43**, 6881–6893.
- 6 W. Y. Seow and C. A. E. Hauser, *Mater. Today*, 2014, **17**, 381–388.
- 7 L. J. Dooling and D. A. Tirrell, in *Monographs in Supramolecular Chemistry No 11*, eds. X. J. Loh and O. A. Scherman, Royal Society of Chemistry, London, 2013, pp. 93–124.
- 8 E. R. Draper and D. J. Adams, *Chem.*, 2017, **3**, 390–410.
- 9 L. Adler-Abramovich, L. Vaks, O. Carny, D. Trudler, A. Magno, A. Caflish, D. Frenkel and E. Gazit, *Nat. Chem. Biol.*, 2012, **8**, 701–706.
- 10 R. V. Ulijn, N. Bibi, V. Jayawarna, P. D. Thornton, S. J. Todd, R. J. Mart, A. M. Smith and J. E. Gough, *Mater. Today*, 2007, **10**, 40–48.
- 11 M. Reches, Y. Porat and E. Gazit, *J. Biol. Chem.*, 2002, **277**, 35475–35480.
- 12 E. Gazit, *Prion*, 2007, **1**, 32–35.
- 13 R. Orbach, I. Mironi-Harpaz, L. Adler-Abramovich, E. Mossou, E. P. Mitchell, V. T. Forsyth, E. Gazit and D. Seliktar, *Langmuir*, 2012, **28**, 2015–2022.
- 14 C. Tang, A. M. Smith, R. F. Collins, R. V. Ulijn and A. Saiani, *Langmuir*, 2009, **25**, 9447–9453.
- 15 S. Farrell, D. DiGuseppi, N. Alvarez and R. Schweitzer-

- Stenner, *Soft Matter*, 2016, **12**, 6096–6110.
- 16 D. DiGiuseppi, L. Thursch, N. J. Alvarez and R. Schweitzer-Stenner, *Soft Matter*, 2019, **12**, 6096–6110.
- 17 P. W. J. M. Frederix, R. V. Ulijn, N. T. Hunt and T. Tuttle, *J. Phys. Chem. Lett.*, 2011, **2**, 2380–2384.
- 18 P. W. Frederix, G. G. Scott, Y. M. Abul-Haija, D. Kalafatovic, C. G. Pappas, N. Javid, N. T. Hunt, R. V Ulijn and T. Tuttle, *Nat Chem*, 2015, **7**, 30–37.
- 19 G. Cheng, V. Castelletto, C. M. Moulton, G. E. Newby and I. W. Hamley, *Langmuir*, 2010, **26**, 4990–4998.
- 20 X. Mu, K. M. Eckes, M. . Nguyen, L. J. Suggs and R. Rengyu, *Biomacromolecules*, 2012, **13**, 3562–3571.
- 21 A. M. Smith, R. J. Williams, C. Tang, P. Coppo, R. F. Collins, M. L. Turner, A. Saiani and R. V. Ulijn, *Adv. Matter*, 2008, **20**, 37–41.
- 22 N. A. Dudukovic and C. F. Zukoski, *Langmuir*, 2014, **30**, 4493–4500.
- 23 V. Singh, K. Snigdha, C. Singh, N. Sinha and A. K. Thakur, *Soft Matter*, 2015, **11**, 353–5364.
- 24 S. Roy and A. Banerjee, *Soft Matter*, 2011, **7**, 5300–5308.
- 25 M. Halperin-Sternfeld, M. Ghosh, R. Sevostianov, I. Grogorians and L. Adler-Abramovich, *Chem. Comm.*, 2017, **53**, 9586–9589.
- 26 G. Fichmann, T. Guterman, J. Damson, L. Adler-Abramovich, J. Schmidt, E. Kesselman, L. J. W. Shimon, A. Ramamoorthy, Y. Talmon and E. Gazit, *Sci. Adv.*, 2016, **2**, e1500827.
- 27 A. Baral, S. Roy, A. Dehsorkhi, I. W. Hamley, S. Mohapatra, S. Ghosh and A. Banerjee, *Langmuir*, 2014, **30**, 929–936.
- 28 K. Basu, A. Baral, S. Basak, A. Dehsorkhi, J. Nanda, D. Bhunia, S. Ghosh, V. Castelletto, I. W. Hamley and A. Banerjee, *Chem. Comm.*, 2016, **52**, 5045–5048.
- 29 N. Amdursky, E. Gazit and G. Rosenman, *Adv. Mat.*, 2010, **22**, 2311–2315.
- 30 J. Raeburn, C. Mendoza-Cuenca, B. N. Cattoz, M. A. Little, A. E. Terry, A. Z. Cardoso, P. C. Griffiths and D. J. Adams, *Soft Matter*, 2015, **11**, 927–935.
- 31 K. M. Eckes, X. Mu, M. A. Ruehle, P. Ren and L. J. Suggs, *Langmuir*, 2014, **30**, 5287–5296.
- 32 P. J. Fleming, N. C. Fitzkee, M. Mezei, R. Srinivasan and G. D. Rose, *Prot. Sci.*, 2005, **14**, 111–118.
- 33 M. Aviv, M. Halperin-Sternfeld, I. Grigorians, L. Buzhansky, I. Mironi-Harpaz, D. Seliktar, S. Einac, Z. Nevo and L. Adler-Abramovich, *ACS Appl. Mater. Interfaces*, 2018, **10**, 41883–41891.
- 34 V. Jayawarna, M. Ali, T. A. Jowitt, A. F. Miller, A. Saiani, J. E. Gough and R. V. Ulijn, *Adv. Mat.*, 2006, **18**, 611–614.
- 35 S. Fleming, S. DE\ebnath, P. W. J. M. Frederix, N. T. Hunt and R. V. Ulijn, *Biomacromolecules*, 2014, **15**, 1171–1184.
- 36 S. Toal, D. Meral, D. Verbaro, B. Urbanc and R. Schweitzer-Stenner, *J Phys Chem B*, 2013, **117**, 3689–3706.
- 37 L. A. Nafie, R. K. Dukor and T. B. Freedman, in *Handbook of Vibrational Spectroscopy*, ed. J. Chalmers & Griffiths, P., John Wiley & Son, New York, 2002, pp. 731–744.
- 38 W. Jentzen, E. Unger, G. Karvounis, J. A. Shelnut, W. Dreybrodt and R. Schweitzer-Stenner, *J. Phys. Chem.*, 1995, **100**, 14184–14191.
- 39 A.-M. Fernandez-Escamilla, F. Rousseau, J. Schymkowitz and L. Serrano, *Nat. Biotechnol.*, 2004, **22**, 1302–1306.
- 40 N. A. Dudukovic and C. F. Zukoski, *Soft Matter*, 2015, **11**, 7663–7673.
- 41 H. C. Service, Fmoc-Glycine, [http://www.hanhonggroup.com/nmr/nmr\\_en/00907.html](http://www.hanhonggroup.com/nmr/nmr_en/00907.html).
- 42 N. J. Baxter and M. P. Williamson, *J. Biomolec. NMR*, 1997, **9**, 359–369.
- 43 G. Gonzalez and I. Chavez, *J. Chem. Soc., Faraday Trans. 2*, 1981, **77**, 2231–2236.
- 44 R. Schweitzer-Stenner, A. Hagarman, S. Toal, D. Mathieu and H. Schwalbe, *Proteins Struct. Funct. Bioinforma.*, , DOI:10.1002/prot.24225.
- 45 S. E. Toal, D. J. Verbaro and R. Schweitzer-Stenner, *J Phys Chem B*, 2014, **118**, 1309–1318.
- 46 S. E. Toal, N. Kubatova, C. Richter, V. Linhard, H. Schwalbe and R. Schweitzer-Stenner, *Chem. Eur. J.*, 2015, **21**, 5173–5192.
- 47 J. Graf, P. H. Nguyen, G. Stock and H. Schwalbe, *J. Am. Chem. Soc.*, 2007, **129**, 1179–1189.
- 48 A. Hagarman, T. J. Measey, D. Mathieu, H. Schwalbe and R. Schweitzer-Stenner, *J. Am. Chem. Soc.*, 2010, **132**, 540–551.
- 49 H. T. Tran, X. Wang and R. V Pappu, *Biochemistry*, 2005, **44**, 11369.
- 50 R. Schweitzer-Stenner, *J. Phys. Chem. B*, 2009, **113**, 2922–2932.
- 51 R. Schweitzer-Stenner, A. Hagarman, S. Toal, D. Mathieu and H. Schwalbe, *Proteins*, 2013, **81**, 955–967.
- 52 L. L. Kimtys and V. J. Balevicius, *Adv. Mol. Recog. Interact. Process.*, 1979, **15**, 151–161.
- 53 S. Fleming, P. W. J. M. Frederix, I. R. Sasselli, N. T. Hunt, R. V. Ulijn and T. Tuttle, *Langmuir*, 2013, **29**, 9510–9518.
- 54 R. Schweitzer-Stenner, *Biophys. J.*, 2002, **83**, 332–523.
- 55 R. Schweitzer-Stenner, H. Carson and D. DiGiuseppi, *Vib. Spec.*, 2017, **92**, 251–258.
- 56 T. Measey, A. Hagarman, F. Eker, K. Griebenow and R. Schweitzer-Stenner, *J. Phys. Chem. B*, 2005, **109**, 8195–8205.
- 57 R. Schweitzer-Stenner, F. Eker, Q. Huang and K. Griebenow, *J. Am. Chem. Soc.*, , DOI:10.1021/ja016202s.
- 58 S. Krimm and J. Bandekar, *Adv Protein Chem*, 1986, **38**, 181–364.
- 59 C. Lee and M. Cho, *J. Phys. Chem. B*, 2004, **108**, 20397–20407.
- 60 R. Schweitzer-Stenner, *J. Phys. Chem. B*, 2012, **116**, 4141–4153.
- 61 T. J. Measey and R. Schweitzer-Stenner, *J. Am. Chem. Soc.*, 2011, **133**, 1066–1076.
- 62 S. Ma, X. Cao, M. M., A. Sadik, C. Walkner, T. B. Freedman, I. K. Lednev, R. K. Dukor and L. A. Nafie, *J. Am. Chem. Soc.*, 2007, **129**, 12364–12365.
- 63 D. DiGiuseppi, L. Thursch, N. J. Alvarez and R. Schweitzer-

## ARTICLE

## Journal Name

- Stenner, *Soft Matter*, 2019, **15**, 3418–3431.
- 64 L. A. Nafie, M. R. Oboodi and T. B. Freedman, *J. Am. Chem. Soc.*, 1983, **105**, 7449–7450.
- 65 W. N. Martens, R. L. Frost, J. Kristof and J. T. Klopogge, *J. Raman Spectrosc.*, 2002, **33**, 84–91.
- 66 Y. Zou, K. Razmkhah, N. P. Chmel, I. W. Hamley and A. Rodger, *RSC Adv.*, 2013, **3**, 10854–10858.
- 67 A. A. Profit, V. Felsen, J. Chinwong, E.-R. E. Mojica and R. Z. B. Desamero, *Proteins*, 2014, **81**, 690–703.
- 68 N. A. Dudukovic and C. F. Zukoski, *Soft Matter*, 2014, **10**, 7849–7856.
- 69 A. G. Mailer, P. S. Clegg and P. N. Pusey, *J. Phys. Cond. Mat.*, 2015, **27**, 145102.
- 70 N. V. Ilawe, R. Schweitzer-Stenner, D. DiGiuseppi and B. M. Wong, *Phys. Chem. Chem. Phys.*, 2018, **20**, 18158–18168.

## TOC

The aromatic dipeptide fluorenylmethoxycarbonyl-di-phenylalanine (FmocFF) self-assembles into amorphous oligomers and fibrils.

